Tropical Cyclone Inner-Core Kinetic Energy Evolution

KATHERINE S. MACLAY

Cooperative Institute for Research in the Atmosphere, Colorado State University, Fort Collins, Colorado

MARK DEMARIA

NOAA/NESDIS, Fort Collins, Colorado

THOMAS H. VONDER HAAR

Cooperative Institute for Research in the Atmosphere, Colorado State University, Fort Collins, Colorado

(Manuscript received 25 May 2007, in final form 3 October 2007)

ABSTRACT

Tropical cyclone (TC) destructive potential is highly dependent on the distribution of the surface wind field. To gain a better understanding of wind structure evolution, TC 0–200-km wind fields from aircraft reconnaissance flight-level data are used to calculate the low-level area-integrated kinetic energy (KE). The integrated KE depends on both the maximum winds and wind structure. To isolate the structure evolution, the average relationship between KE and intensity is first determined. Then the deviations of the KE from the mean intensity relationship are calculated. These KE deviations reveal cases of significant structural change and, for convenience, are referred to as measurements of storm size [storms with greater (less) KE for their given intensity are considered large (small)]. It is established that TCs generally either intensify and do not grow or they weaken/maintain intensity and grow. Statistical testing is used to identify conditions that are significantly different for growing versus nongrowing storms in each intensification regime. Results suggest two primary types of growth processes: (i) secondary eyewall formation and eyewall replacement cycles, an internally dominated process, and (ii) external forcing from the synoptic environment. One of the most significant environmental forcings is the vertical shear. Under light shear, TCs intensify but do not grow; under moderate shear, they intensify less but grow more; under very high shear, they do not intensify or grow. As a supplement to this study, a new TC classification system based on KE and intensity is presented as a complement to the Saffir–Simpson hurricane scale.

1. Introduction

Surface wind structure is a significant component of tropical cyclone (TC) destructive potential. For a large storm, compared to a small storm of equal intensity, not only will the wind damage be greater but such a storm will also generate a larger storm surge. Storm surge is a very serious threat to coastal regions often causing greater damage than the winds (AMS 1993). This was dramatically demonstrated by Hurricane Katrina (2005), which caused unprecedented storm surge damage to portions of Louisiana and Mississippi yet was rated only as a category 3 on the Saffir–Simpson hurricane scale (SSHS) at landfall.

Tropical cyclone size can vary greatly, as is well illustrated by Hurricanes Charley (2004) and Wilma (2005). Both began as small-sized storms that intensified rapidly to major hurricane intensity. However, while Charley remained small throughout its evolution, Wilma experienced substantial structural growth. At their respective Florida landfalls, Charley had a radius of maximum wind (RMW) of ~3 nautical miles (5.6 km) and an intensity of 64 m s^{-1}, and Wilma had an RMW of ~30 nautical miles (55.6 km) with an intensity of 54 m s^{-1} (Fig. 1). These storms, while unique in their own right, are not anomalous with respect to their structural changes.

TC intensity has consistently been measured by either maximum sustained wind or minimum central

Corresponding author address: Katherine S. Maclay, CIRA/Colorado State University, Fort Collins, CO 80523-1375.
E-mail: maclay@cira.colostate.edu

DOI: 10.1175/2008MWR2268.1

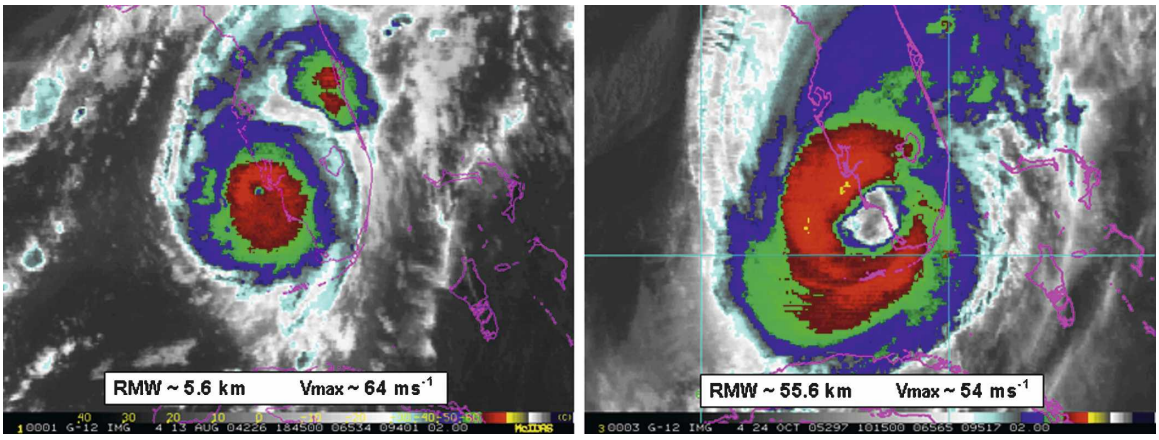

FIG. 1. GOES infrared image of Hurricanes (left) Charley (2004) and (right) Wilma (2005) at the time of their respective Florida landfalls.

pressure. Overall size has been determined from parameters such as radius of outer closed isobar or radius of gale-force winds, while inner-core size is traditionally given by the eye diameter and RMW. Strength has been measured and defined in a great variety of ways but is generally considered a measure of the areal extent of some defined wind speed.

In this study, the wind structure is determined from 0- to 200-km wind fields of TCs from 1995 to 2005, derived from aircraft flight-level data. Intensity is defined as the maximum wind speed ($m\,s^{-1}$) from objective analyses of flight-level data (unless otherwise specified). The wind structure parameter is the low-level area-integrated kinetic energy (KE). This integrated KE depends on both storm intensity and wind structure. To isolate the wind structure component, the KEs for the entire dataset are first plotted versus intensity, revealing a general trend of mean KE compared to intensity. The KE deviations from the mean KE/maximum wind relationship are then used as a measure of the wind structure. For convenience, the KE deviations are referred to as a measure of storm size [storms with greater (less) KE for their given intensity are considered large (small)].

The KE deviation parameter is probably more closely related to what has been called "strength" in previous studies (e.g., Merrill 1984). However, strength is also commonly used as a synonym for intensity, so that terminology was not used here. The KE deviation measure of storm size is correlated with the more traditional measure of storm size as measured by the radius of gale-force winds (R34). To quantify this relationship, the values of R34 for the total aircraft analysis sample were obtained from the National Hurricane Center (NHC) best track for cases since 2004, and from the NHC advisories prior to 2004 (NHC did not create best-track radii until 2004). A correlation between KE deviation values and similarly calculated R34 deviation values give a correlation coefficient of 0.6, indicating a weak but nonnegligible relationship between the KE measure of size used in this study and the more traditional size measure. All references to size and growth in this study will be with respect to the KE deviations. So, a storm is considered growing if its KE deviations increase with time and is considered not growing if the deviations decrease. These KE deviations are then used to identify growing and nongrowing cases.

Previous studies focused on the relationship between TC intensity and size or strength. Such studies have shown that typically inner-core intensity change precedes change in the storm outer-core winds (Weatherford and Gray 1988a,b; Merrill 1984; Croxford and Barnes 2002). Kimball and Mulekar (2004) observed that weakening storms tend to be large, intense, and highly organized as they are often more mature, whereas intensifying storms, often early in their life cycle, are generally small and less intense. Recurvature and extratropical transition, a common occurrence in Atlantic Ocean TCs (Hart and Evans 2001), have been found to affect TC size and intensity by generally decreasing intensity and increasing size (Sinclair 2002; Jones et al. 2003).

Internal dynamics and synoptic forcing have been suggested as key factors in determining TC size (Cocks and Gray 2002) and intensity (Wang and Wu 2004). The model- and theory-based studies of Challa and Pfeffer (1980), Shapiro and Willoughby (1982), and Holland and Merrill (1984) provide some useful insights into the possible mechanisms for TC intensity and size change. Cumulatively, they suggest that upper- and lower-level forcing via heat and momentum sources may be instrumental in TC size change. To further investigate these theories as well as to determine

other mechanisms for growth, a statistical analysis of our KE cases was performed, as described below.

The individual cases are sorted into six groups defined by the storm's state of intensification and size change. Geostationary Operational Environmental Satellite (GOES) infrared data for each group are examined to determine if there are convective differences between the groups. Microwave satellite data are also examined for some cases to better identify the eyewall structure. The environmental conditions most significant for each group are analyzed using National Centers for Environmental Prediction (NCEP) reanalysis fields. Special emphasis is given to the anomalous cases in which a storm intensifies and grows or weakens and does not grow.

As an offshoot of this research, a new hurricane scale based on integrated KE and intensity is proposed. The scale is developed as a complement to the SSHS and has the benefit of incorporating storm size. The KE scale and SSHS are compared by looking at all U.S. landfalling hurricanes from 1995 to 2005.

2. Data sources

The primary dataset for this study is the objectively analyzed aircraft reconnaissance flight-level data, which are used to calculate KE, as described in section 3. A variety of auxiliary datasets are used to analyze storm attributes and conditions. Satellite data include Geostationary Operational Environmental Satellite (GOES) infrared measurements and the Special Sensor Microwave Imager (SSM/I) and Special Sensor Microwave Imager/Sounder (SSMIS) microwave imagery. The National Centers for Environmental Prediction reanalysis data (Kistler et al. 2001; Toth et al. 1997) provide storm synoptic environmental conditions. Finally, assorted integrated storm and storm environment variables from the Statistical Hurricane Intensity Prediction Scheme (SHIPS) model predictors, GOES infrared data, and the aircraft reconnaissance data provide a description of a variety of attributes of each storm and its environment.

The 0–200-km wind fields of Atlantic and eastern Pacific Ocean TCs from 1995 to 2005 on a cylindrical grid (Δr = 4 km; $\Delta\theta$ = 22.5°) are determined from an objective analysis of the U.S. Air Force Reserve aircraft reconnaissance data as described by Mueller et al. (2006). The 0–200-km radial domain is chosen to match the standard length of the flight legs for the aircraft reconnaissance flights. To better capture the time evolution of the KE, the objective analysis used data composited over 6-h intervals instead of the 12-h intervals used by Mueller et al. The 124 storms for this study yield a total of 1244 flight-level wind field analyses. The maximum flight-level winds from the objective analyses are also determined to investigate the relationships between intensity and size. Furthermore, variables to estimate the eye and storm sizes, respectively, are derived from the aircraft reconnaissance data. These variables are the radius of maximum symmetric tangential wind (RMSTW) and the tangential wind gradient outside the RMW (TWG).

The convective profiles and inner-core convection are investigated using 4-km resolution, storm-centered, digital GOES infrared (IR) satellite imagery (Kossin 2002). The azimuthally averaged, radial profile data extends from 0–500 km from storm center and includes both the brightness temperatures T_b and the azimuthal standard deviations of the T_b at each radius, which is a measure of the convective asymmetry. Additionally, the GOES IR data are used to derive a variable to measure the inner-core convection. The variable (CONV) is the percent area in the 50–200-km radial band with T_b below −40°C.

Imagery from the SSM/I 85-GHz and SSMIS 91-GHz horizontally polarized channels are used to identify secondary eyewall formation and eyewall replacement cycles in selected storms in section 4. [This imagery was retrieved from the Naval Research Laboratory (NRL) Monterey Marine Meteorology Division TC Web page at http://www.nrlmry.navy.mil/tc_pages/tc_home.html.]

Variables related to the location and synoptic scale environment are acquired from the SHIPS predictor variables (DeMaria et al. 2005). These variables provide integrated measures of the storm's thermodynamic, dynamic, and internal conditions. The latitude (LAT), longitude (LON), sea surface temperature (SST), ocean heat content (OHC), magnitude of the deep shear (200–800-km radial average) (SHR), environmental 850-hPa vorticity (0–1000-km average) (VORT), and the 150-hPa temperature (T150), which gives an estimate of the tropopause height, provide information about the storm environment. The 100–600-km average, 200-hPa relative eddy momentum flux convergence variable (REFC) is a good indicator of trough interactions (DeMaria et al. 1993; Holland and Merrill 1984; Molinari and Vollaro 1989). The storm latitude and longitude were obtained from the NHC best-track data and were utilized to calculate storm speed (SPD) and direction.[1]

From the datasets described above, a broad selection of integrated variables encompassing information about the storm and storm environment was statisti-

[1] The direction variable revealed no statistically significant information and is therefore not presented.

TABLE 1. Storm and storm environment variables used in this study.

Variable name	Description	Units and scaling	
SST	Reynolds SST	°C	SHIPS model
T150	150-hPa temperature	°C	
LAT	Latitude	°N	
LON	Longitude	°W	
SHR	850–200-hPa shear magnitude	$m\ s^{-1}$	
VORT	850-hPa vorticity	$s^{-1} \times 10^5$	
REFC	200-hPa relative eddy momentum flux convergence	$m\ s^{-1}\ day^{-1}$, 100–600 km average	
OHC	OHC derived from satellite altimetry	$kJ\ cm^{-2}$	
SPD	Storm speed	$m\ s^{-1}$	
CONV	% area r = 50–200 km with brightness temperature <-40°C	%	GOES
RMSTW	Radius of max symmetric tangential wind	km	Aircraft reconnaissance
TWG	Tangential wind gradient outside the radius of max wind	$100 \times m\ s^{-1}\ km^{-1}$	

cally analyzed to determine the variables' relative importance in TC size change. A subset of these was found to be significantly related to size changes, which are listed in Table 1 by variable name, description, and units and scaling.

In addition to the integrated synoptic variables listed in Table 1, some of the basic synoptic fields from the NCEP reanalysis data were also examined. These include the upper-level (200 hPa) and lower-level (850 hPa) horizontal wind fields, the 850–200-hPa shear, and the 700-hPa temperature advection fields on 31° by 41° latitude/longitude storm-centered grids.

3. Kinetic energy climatology and hurricane scale

As discussed in previous sections, the KE of the wind field is likely an important factor in determining TC-related destruction. This section will 1) describe a method to estimate KE from winds measured during routine reconnaissance of Atlantic and eastern Pacific TCs, 2) describe the climatology of this KE calculation, 3) show how estimated KE is related to TC destruction, and 4) compare it with the SSHS.

To estimate KE from a single level, some assumptions are necessary. First, consider the storm to be a thin disk within a constant radius and depth interval. The total KE is found by integrating the kinetic energy for a single air parcel over the volume of the disk:

$$\mathrm{KE} = \int_{z_1}^{z_2} \int_0^{2\pi} \int_0^R \frac{1}{2} \rho (u^2 + v^2) r \, dr \, d\theta \, dz, \qquad (1)$$

where u is radial wind, v is tangential wind, ρ is air density, r is radius, θ is azimuth, and z is height. The aircraft reconnaissance flight-level winds are assumed to be representative of the storm structure over a 1-km depth and are usually available out to a 200-km radial distance from storm center. A constant density is assumed because the variation in air density within this volume is small. Therefore, the KE equation becomes

$$\mathrm{KE} = \frac{\rho_o \Delta z}{2} \int_0^{2\pi} \int_0^R (u^2 + v^2) r \, dr \, d\theta, \qquad (2)$$

where ρ_o is assigned a value of 0.9 $kg\ m^{-3}$ (a typical air density at 700 hPa, the standard flight level for hurricane reconnaissance flights). Using (2), KE is calculated for all analyses in the dataset.

To determine how storm energy evolves during intensification, the KEs (J) are plotted versus the maximum analyzed winds ($m\ s^{-1}$) in Fig. 2. From the basic definition of kinetic energy, one would expect a storm's kinetic energy to increase with the square of the maximum wind. However, the integrated KE also depends on the wind distribution, so it would not necessarily be proportional to the square of the maximum wind. A best fit applied to the data reveals a power series relationship:

$$\mathrm{KE} = 3 \times 10^{13} (V_{\max})^{1.872}. \qquad (3)$$

The variance explained, R^2, for this best fit is 82%. Thus, KE increases with nearly the square of the maximum winds. It should be noted that the mean KE-intensity relationship does not describe the evolution of KE for individual storms and there is considerable variability in KE for a given intensity. The KE evolution through the life cycle of individual storms is investigated more thoroughly in section 4.

The highly active TC seasons of 2004 and 2005 and the devastation caused to Louisiana and Mississippi by Hurricane Katrina have sparked increased concern over the effectiveness of the SSHS in accurately alert-

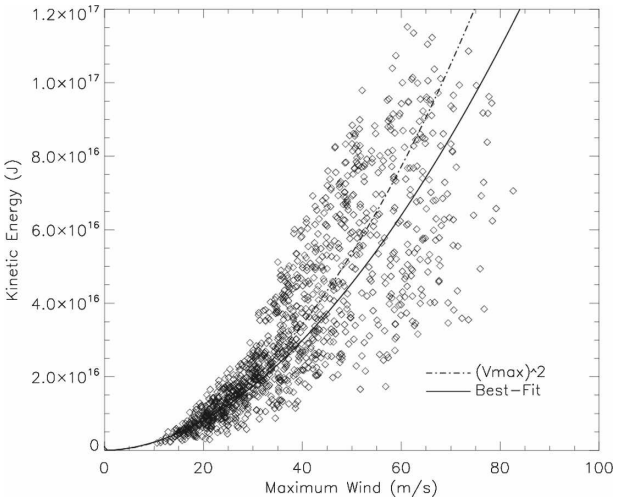

FIG. 2. KE vs intensity (V_{max} from the aircraft reconnaissance analyses).

ing the public to a storm's potential danger. Several studies such as Kantha (2006) and Powell and Reinhold (2007) have suggested replacing the SSHS with improved scales. Kantha proposes a set of dynamic-based continuous scales for intensity and wind-damage potential, similar to those used for earthquakes. It gives better accuracy by incorporating size into the scaling and retains a separate measure for intensity, which would be useful for small, intense storms. These calculations for the wind damage potential use the cube of the maximum wind, which in practice might be somewhat inaccurate due to the underlying uncertainties in the ability to estimate maximum wind (Brown and Franklin 2004). Also, a continuous and highly nonlinear scale would be valuable for sophisticated users, but it might be problematic for conveying information to the general public. Powell and Reinhold proposed wind and storm surge destructive potential scales based on integrated kinetic energy (IKE). Their IKE is calculated quite similarly to the KE in this study but over a larger area ($8° \times 8°$ grid) using the H*Wind (Powell et al. 1998) analysis fields as opposed to the aircraft reconnaissance flight-level winds. Using area-integrated kinetic energy to estimate storm destructive potential takes into account both intensity and size. The SSHS only takes into account intensity. Incorporating size should provide further insight into potential storm damage by severe winds, intense rain, and storm surge. Much of the beauty and success of the SSHS is in its simplicity. In an effort to preserve the established usefulness of the SSHS yet account for aspects of size, the KE from this study is used to form a classification to complement the SSHS. This KE scale is designed to be used in conjunction with the SSHS for ease of implementation.

TABLE 2. The SSHS and the proposed kinetic energy hurricane scale (KEHS).

Category	SSHS (V_{max}) ($m\ s^{-1}$)	Percentage (%)	KEHS ($\times 10^{16}$ J)
0	17–32	53.0	<2.84
1	33–42	24.4	2.84–5.35
2	43–49	10.9	5.35–7.09
3	50–58	6.5	7.09–8.56
4	59–69	4.2	8.56–10.0
5	≥70	1.1	>10.0

To illustrate the potential for a new scale, a system of six categories is defined ranging from 0 to 5, where category 0 represents tropical storms on the SSHS. The percentage of storms corresponding to each SSHS category is determined from the 1947–2004 NHC best-track data. The thresholds for the KE hurricane scale categories are chosen by applying these same percentages to the KE climatology dataset. Table 2 outlines the SSHS categories, their corresponding historical distributions, and the analogous KE hurricane scale categories.

To compare these scales, consider the 1995–2005 U.S. landfalling hurricanes. Table 3 shows, for each storm, the date and time of the objective analysis closest to the storm's landfall time, the time difference between the analysis and the actual landfall, the intensity from the analysis, the official NHC intensity at landfall, the SSHS category, the KE calculated from the analysis, and the KE scale category. Storms with two landfalls, such as Hurricane Katrina, which crossed Florida before making its final landfall in Louisiana and Mississippi, are indicated by I for the first landfall and II for the second.

The KE values for the analysis closest in time to landfall for each storm are plotted against the official NHC intensities ($m\ s^{-1}$) in Fig. 3. The vertical dotted lines mark thresholds for the SSHS categories and the horizontal dotted lines are thresholds for the KE hurricane scale categories. Observe first the data points for Hurricanes Katrina (2005) and Ivan (2004). On the SSHS, Katrina made landfall on the Louisiana–Mississippi border as a category 3; however, the KE scale measures the storm as an impressive category 5. Similarly, Ivan was nearly a KE category 5 at landfall, and it too was an SSHS category 3. Katrina caused an estimated $75 billion (Knabb et al. 2006) and Ivan an estimated $14.2 billion (Franklin et al. 2006) in damage. These were the two most costly storms in the United States from 1995 to 2005, yet they were not the most intense to make U.S. landfall for this period. However, for both of these storms, much of the damage was a

TABLE 3. Data for all U.S. landfalling hurricanes (1995–2005) at approximately the time of their respective landfall. A negative time before landfall indicates that the analysis is from after landfall.

Storm name	Avg analysis time (LT)	Time before landfall (h:min)	Analysis V_{max} (m s^{-1})	NHC V_{max} (m s^{-1})	SSHS category	KE ($\times 10^{16}$ J)	KEHS category
Erin I 1995	0449 2 Aug	1:26	39.0	38.6	1	3.35	1
Erin II 1995	1436 3 Aug	1:24	43.8	38.6	1	2.52	0
Opal 1995	0128 4 Oct	20:32	43.2	51.4	3	4.47	1
Bertha 1996	2052 12 Jul	−0:52	46.4	46.3	2	4.07	1
Fran 1996	2136 5 Sep	2:54	54.6	51.4	3	8.83	4
Danny I 1997	0421 18 Jul	4:39	34.9	33.4	1	1.23	0
Danny II 1997	1601 19 Jul	1:59	31.1	33.4	1	1.45	0
Bonnie 1998	0457 27 Aug	−0:57	38.9	48.9	2	5.34	1
Earl 1998	0415 3 Sep	1:45	38.7	36.0	1	3.02	1
Georges I 1998	2312 25 Sep	−7:42	42.7	46.3	2	5.52	2
Georges II 1998	2104 27 Sep	14:26	41.1	46.3	2	6.03	2
Bret 1999	1623 22 Aug	7:37	59.9	51.4	3	3.96	1
Floyd 1999	0524 16 Sep	1:06	50.1	46.3	2	6.92	2
Lili 2002	1020 3 Oct	2:40	45.9	41.2	1	5.27	1
Claudette 2003	1354 15 Jul	1:36	40.6	41.2	1	2.73	0
Isabel 2003	1551 18 Sep	1:09	57.3	46.3	2	8.10	3
Charley I 2004	1653 13 Aug	3:52	56.4	64.3	4	2.45	0
Charley II 2004	1009 14 Aug	5:51	38.8	33.4	1	3.29	1
Gaston 2004	2119 28 Aug	16:41	28.2	33.4	1	1.50	0
Frances 2004	0511 5 Sep	−0:41	48.6	46.3	2	7.02	2
Ivan 2004	1946 15 Sep	11:04	63.3	54.0	3	9.99	4
Jeanne 2004	0501 26 Sep	−0:59	48.5	54.0	3	7.02	2
Dennis 2005	2021 10 Jul	−0:51	55.5	54.0	3	4.04	1
Katrina I 2005	2047 25 Aug	1:43	35.5	36.0	1	1.99	0
Katrina II 2005	1444 29 Aug	0:01	62.5	54.0	3	11.35	5
Rita 2005	2107 23 Sep	10:33	57.5	53.6	3	9.56	4
Wilma 2005	0418 24 Oct	6:12	59.2	54.0	4	8.76	4

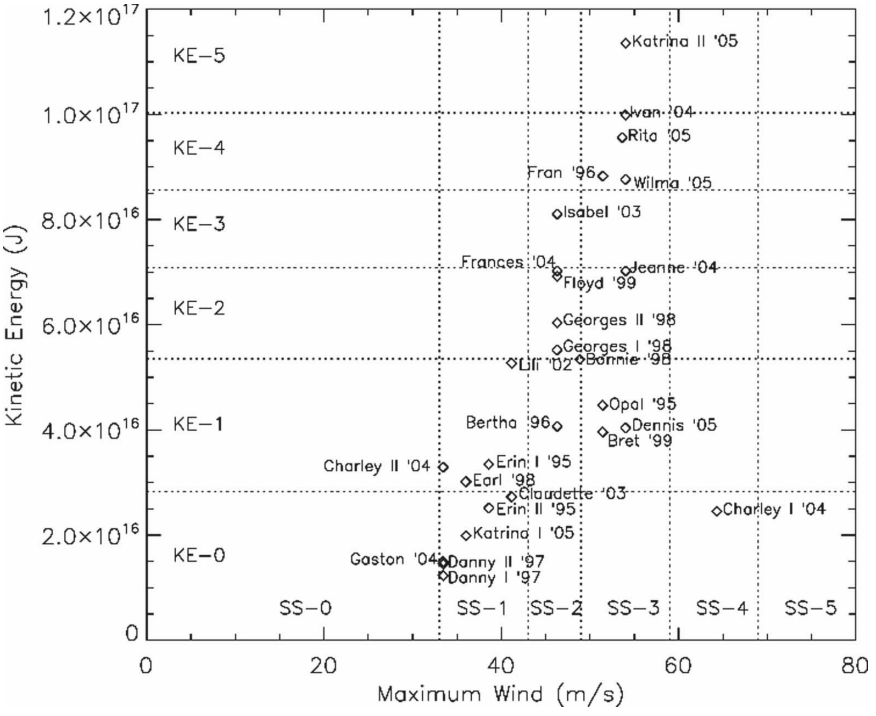

FIG. 3. The approximate KE vs V_{max} as reported by NHC at landfall for all U.S. landfalling hurricanes from 1995 to 2005.

result of storm surge. Thus, the KE scale appears to provide additional information about a hurricane's potential for damage that is not available solely from intensity.

The main weakness of the KE and intensity scales is that they do not accurately represent the destructive potential of small, intense storms. Hurricane Charley (2004), which caused an estimated $14 billion in damage, is a good example. At its first landfall in Punta Gorda, Florida, the storm measured a category 4 on the SSHS, but it was a KE category 0. At its second landfall in Myrtle Beach, South Carolina, it had weakened to a SSHS category 1, yet increased to a KE category 1. At first landfall, the storm was an extremely intense, compact system. While it contained very strong winds, they were confined to within 6 nautical miles (11.1 km) of the storm center based on the flight-level winds. Such a small RMW makes it impossible to adequately resolve the high-wind features near the eyewall even in the reconnaissance data (which has a 4-km resolution). At the second landfall, it had weakened with respect to its maximum sustained winds but had become a larger system with fairly high winds covering a greater area, resulting in an increased KE. The most significant damage occurred during initial landfall and was caused by extreme winds rather than storm surge, of which there was a minimal amount. Powell and Reinhold (2007) attempt to account for these small, intense storms by weighting storms with winds ≥ 55 m s^{-1} more heavily in their scale, yet they still noted similar weaknesses in representing the destructive potential of small, intense storms such as Charley. A better understanding of wind destructive potential is likely necessary to adjust these scales to account for such storms. An alternate approach is to simply use the SSHS and KE scales in conjunction, as both provide valuable information about storm destructive potential.

4. KE evolution

While the overall evolution in KE with respect to intensity is generally defined by the power series curve (3), individual storms rarely evolve in this manner. This is best illustrated by the time evolution of individual storm KE deviations (KE′) from the mean curve as a function of intensity. The KE′ are calculated as the difference between the measured and expected KE for the storm's intensity from (3). A zero value in KE′ indicates that the storm has the expected KE for its intensity and lies on the mean curve described by (3) and shown in Fig. 2. As described previously, increasing KE′ implies storm growth and decreasing KE′ implies the storm is not growing relative to its intensity evolution. The KE′ evolution is examined for all storms with at least three associated aircraft analyses, of which there are 97 cases.

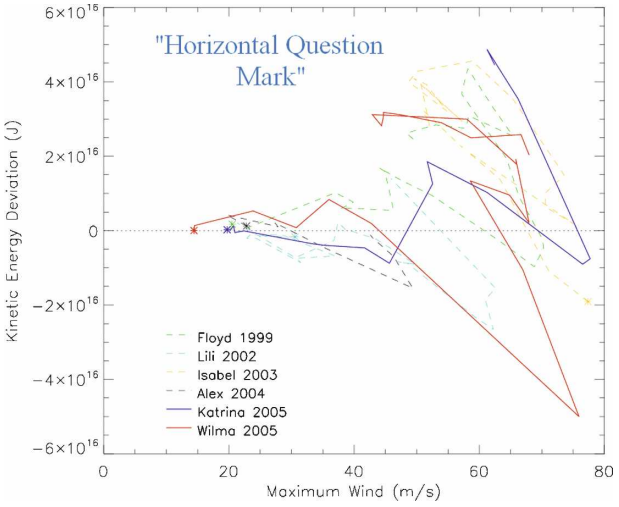

FIG. 4. Time evolution of KE′ vs V_{max} for six selected storms. Note in particular the plots for Hurricanes Katrina and Wilma.

a. Horizontal question mark evolution

Extensive review of the KE′ evolution plots reveal some common characteristics. TCs more commonly intensify and decrease in KE′ (i.e., do not grow) or decrease in intensity and increase in KE′ (i.e., grow). The opposites occur less frequently. In fact, a unique evolution in intensity and structure is apparent, which will be referred to as the "horizontal question mark" evolution for simplicity. Examples of this can be seen in Fig. 4, which shows the time evolution of KE′ versus V_{max} plots for six TCs. Storms that had reconnaissance data extending through the greater part of the storm's evolution, such as Hurricanes Katrina and Wilma (2005), showed this pattern most commonly. This evolution suggests that as a storm begins to intensify, there is often a modest decrease in KE′, but as a stage of more rapid intensification is reached, the KE′ decreases substantially. Once reaching peak intensity and weakening begins, the KE′ often increases. These findings comply with previous studies by Weatherford and Gray (1988a,b) and Merrill (1984), which suggested TCs generally do not intensify and grow simultaneously, as well as Kimball and Mulekar's (2004) findings that generally weakening storms are large and intensifying storms small.

b. Eyewall replacement cycles

Examining the plots of KE′ versus V_{max} in combination with microwave and IR for several major hurri-

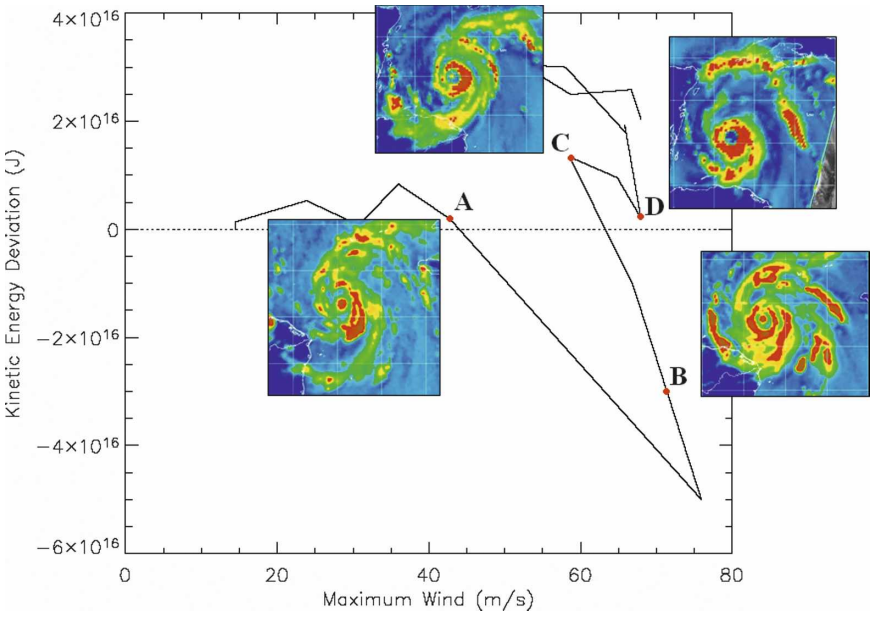

FIG. 5. The KE′ vs V_{max} evolution of Hurricane Wilma with relevant microwave imagery overlaid to illustrate the occurrence of an eyewall replacement cycle.

canes revealed that secondary eyewall formation and eyewall replacement cycles (ERCs) (Willoughby et al. 1982) are often associated with nearly discrete KE′ changes. As the secondary eyewall begins to dominate, its larger size results in a KE′ increase, even though the V_{max} has often weakened during this process. The new, larger eye may then become more organized, intensify, and contract completing the ERC. Thus, an intensity increase and KE′ decrease is seen.

Hurricane Wilma (2005) had a dramatic ERC early in the storm's lifetime. Figure 5 shows the KE′ evolution with respect to intensity for Wilma with corresponding microwave imagery overlain (points A–D). Wilma formed in the Caribbean (point A in Fig. 5) and very quickly intensified into an extremely small, intense TC (point B in Fig. 5). Its tiny eye then became encompassed by a much larger secondary eyewall. The small eye broke down, leaving the larger eye in its place (point C in Fig. 5), which then proceeded to organize and intensify (point D in Fig. 5). The storm's development, as shown in the microwave imagery, is clearly evident in the KE′ and intensity evolution. As the storm developed to its peak intensity, the KE′ decreased (A–B). During the ERC the intensity decreased, but the KE′ increased (B–C) as the larger eye formed. Finally, as the new eye began to contract, the storm experienced moderate intensification and a KE′ decrease (C–D).

Hurricane Wilma's ERC illustrates a discrete growth process common to strong TCs. During the ERC, the storm initially loses intensity as the inner eyewall breaks down and is replaced by an existing secondary eyewall. The new eye may contract as the storm reintensifies, but it generally remains larger than the previous eye. This is a primary mechanism for storm growth and was also seen in several other storms including Ivan (2004) and Floyd (1999).

c. *Intensity change/size change regimes*

To confirm the prevalence of these evolutional tendencies and to facilitate further analysis of storm structural evolution, time tendencies of intensity and KE′ are calculated. The time tendencies are calculated using centered time differences, with one-sided differences at the beginning and end of each time series. The reconnaissance analysis times are unequally spaced in time so the tendencies are normalized to a 24-h period, denoted by ΔV_{max} and ΔKE′. Also, ΔKE′ and ΔV_{max} values are only used for analyses at least 3 h but less than 24 h apart. This restriction avoids unrealistic values for the 24-h intensification or growth when the aircraft reconnaissance analyses are too close or far apart. Eastern Pacific storms are excluded from this portion of the analysis because of the basins' limited availability of aircraft data. This should not affect the results, as this eliminates only a few storms, leaving 91 storms and a total of 1123 analyses for this portion of the study.

The ΔV_{max} and ΔKE′ values are sorted by intensity change, and three groups are defined: the lower third represents weakening storms (W), the upper third in-

TABLE 4. The percentage of analyses associated with each intensification/growth regime.

	Weakening	Maintaining	Intensifying
Nongrowing	7.3%	13.9%	24.3%
Growing	26.1%	19.4%	9.0%

tensifying storms (I), and the middle third storms approximately maintaining intensity (M). The weakening, maintaining, and intensifying groups are split into growing (i.e., positive $\Delta KE'$) and nongrowing (i.e., negative $\Delta KE'$) groups, represented by G and NG, respectively. Table 4 shows that weakening storms are more often growing, and intensifying storms are more often not growing. This not only supports previous studies but also provides a quantitative measure of the preliminary investigation of the KE'/V_{max} evolution shown in Fig. 4 (horizontal question mark). The growing, weakening (GW) and nongrowing, intensifying (NGI) cases in Table 4 correspond to negative slopes in the V_{max}–KE' phase space diagram in Fig. 4, and the nongrowing, weakening (NGW) and growing, intensifying (GI) cases correspond to positive slopes. The maintaining intensity cases (GM, NGM) have small slopes. In the large sample, 50.4% of the cases have negative slopes, while only 16.3% are positively sloped.

5. Conditions associated with structure changes

A climatology of TC growth with respect to intensification suggests that generally weakening storms grow and intensifying storms do not grow. While these observations are interesting, they are not all that enlightening. Using the available data divided into the six groups introduced above (GW, NGW, GI, NGI, GM, and NGM), the following sections discuss mechanisms for TC growth.

a. Basic storm and storm environmental conditions

A first step is to determine characteristics and basic environmental conditions common to each of the six groups in Table 4. Utilizing the objectively analyzed reconnaissance data, GOES IR brightness temperature (T_b) profile data, and the SHIPS model data records, information about both the storm at the time of each analysis and the associated environmental conditions is retrieved and sorted into arrays based on the group classifications.

How the environmental conditions for the G versus NG storms in each intensification scenario compare is of particular interest. To determine these relationships, the difference in the means of G from NG storms is calculated and is nondimensionalized by normalizing by the standard deviations of each variable. Statistical analysis using the Student's *t* test is employed to determine the probability that a given variable is significantly different for G versus NG storms in each intensification regime. A 95% significance threshold isolates variables worthy of further investigation. Table 5 shows the mean value for each variable in each group. The shading indicates where the 95% significance threshold has been met.

TABLE 5. Mean values for the storm and storm environment variables are shown in this table. The boldface values indicate those scenarios that showed a 95% statistically significant difference.

	Weakening		Intensifying		Maintaining	
	NGW	GW	NGI	GI	NGM	GM
LAT	**27**	**23.4**	**21.7**	**25.7**	**25.6**	**24.4**
LON	76.7	74.5	**74.7**	**78.8**	**72.8**	**75.3**
SST	**28.1**	**28.5**	28.8	28.6	**28.1**	**28.7**
OHC	**40.4**	**52.8**	**63.2**	**54.2**	**44.1**	**54.9**
T150	**−65.2**	**−65.7**	**−66.3**	**−65.5**	−65.6	−65.8
SHR	**9.8**	**8.4**	**7.6**	**8.5**	**9.2**	**7.6**
VORT	**23.8**	**34.7**	40.1	44.2	29.5	25.5
REFC	3.0	3.5	**3.0**	**4.4**	3.3	3.5
SPD	**3.6**	**4.3**	4.2	4.0	**4.3**	**3.8**
CONV	**52.8**	**67.4**	**73.9**	**65.3**	62.6	66.7
RMSTW	**91.0**	**60.1**	**58.7**	**81.8**	77.1	81.7
TWG	**−9.4**	**−22.2**	**−22.1**	**−13.3**	−14.4	−15.2

While usually storms either intensify or grow, but do not do both simultaneously, occasionally storms weaken and do not grow, or sometimes they intensify and grow (these are termed the "anomalous" storms). From the results shown in Table 5 some prevalent conditions are associated with anomalous structural development.

Consider GI storms in comparison with the typical NGI storms. These storms tend to be located at higher latitudes, farther west, with lower tropopause heights (warmer T150). They are positioned over lower ocean heat content waters and experience higher shear and eddy momentum flux convergence suggesting trough interaction. They have less inner-core convection, a larger radius of maximum symmetric tangential wind, and a smaller tangential wind gradient outside the RMW. The higher shear and momentum fluxes indicate that trough interaction is important for growth in intensifying storms. A numerical modeling study by Kimball and Evans (2002) showed that in idealized scenarios, trough interaction results in increased TC size and strength but in decreased maximum intensity in comparison to a simply shear-influenced storm. In the real atmosphere, a trough may supply the extra angular momentum needed to support simultaneous intensification and growth. Also, many of the conditions nor-

mally associated with intensification (low shear, warm SST, and high OHC) are less for GI cases. This suggests that in environments favorable for intensification, changes are more confined to the inner core and have less impact on storm size.

The second anomalous case is NGW storms. Relative to GW cases, these storms generally move more quickly, are located at higher latitudes, have lower tropopause heights, and are positioned over cooler SSTs and lower OHC waters. They experience greater shear and lower values of environmental vorticity. Less inner-core convection, a larger inner core, and a smaller tangential wind gradient outside the RMW are also common to these storms. These characteristics are indicative of storms in a less favorable environment preventing the normal growth seen in weakening storms. Generally, those factors that contribute to growth in an intensifying storm restrict growth in weakening storms. In these cases, the conditions may be so hostile that the storm is on its way to final dissipation or extratropical transition. Keeping this in mind, greater focus will be given to GI storms from this point forward. To better understand these processes, a more in-depth study of the convection and synoptic environments is necessary.

b. Convective profiles

For a better understanding of the structure of inner- and outer-core heating in the different storm types, consider the GOES IR brightness temperature (T_b) and standard deviations in T_b radial profiles. High clouds from more intense convection measure as colder T_bs, so the T_b profiles reveal more information about the storm convective structure. The standard deviation in T_b provides a measure of the asymmetry of convection, where higher values indicate greater convective asymmetry. It is noted that a cirrus canopy from a convectively active eyewall may obscure rainband convection in the infrared imagery. However, the absence of cold cloud-top temperatures in the infrared imagery is a guarantee that there is no underlying deep convection.

Although the T_b profiles for intensifying storms do not show significant differences in their means, there are some interesting features (Fig. 6, top). At the storm center, the cloud-top temperatures are nearly the same, but the T_b profiles diverge noticeably outward through the eyewall. The NGI storms exhibit colder cloud tops through the eyewall, indicating an increased convective region. The GI storms, on the other hand, show a flatter, less convective T_b profile through the eyewall.

The T_b standard deviation profiles for intensifying storms exhibit significant differences for GI versus NGI storms (Fig. 6, bottom). Near the storm center (6–10 km), NGI storms show greater convective asymmetry,

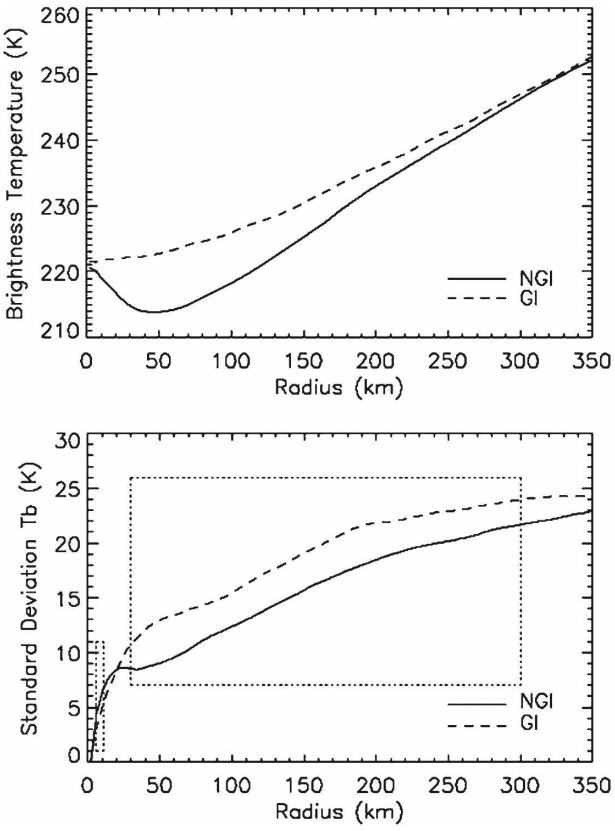

FIG. 6. Mean radial profiles of the (top) (GOES IR brightness temperatures and (bottom) standard deviation in brightness temperatures for intensifying storms. The boxes indicate the areas where the G vs NG storm profiles showed statistically significant differences.

but near the eyewall and extending out to the outer rainbands (30–330 km), GI storms are more convectively asymmetric. This suggests that GI storms have more heating occurring outside the eyewall and extending into the rainbands than NGI storms.

c. Synoptic environments

Using NCEP reanalysis data corresponding to each aircraft reconnaissance analysis, a composite analysis of the storm-centered horizontal wind fields is created for pressure levels of 200, 500, 700, and 850 hPa. The magnitude of the 850–200-hPa shear vectors is calculated using the composite 200-hPa and 850-hPa horizontal winds. The 2D wind field and deep-shear plots provide a more detailed view of the synoptic conditions associated with each storm type.

Consider first the 200-hPa, 850-hPa, and deep-shear fields for intensifying storms. The 200-hPa mean wind fields for both NGI and GI (Fig. 7) storms show evidence of the upper-level anticyclones that customarily

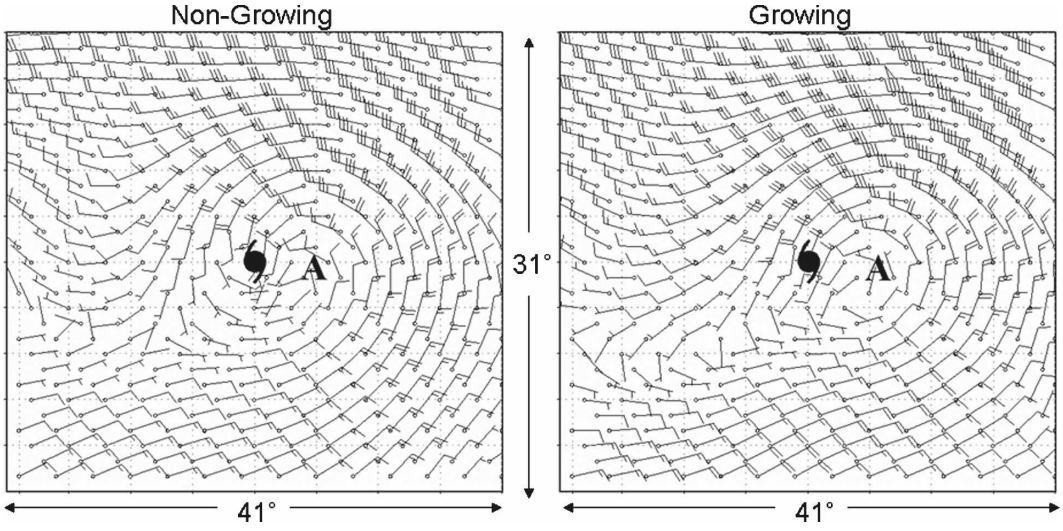

FIG. 7. The 200-hPa mean wind fields (kt) for intensifying storms. (left) The composite field for the nongrowing storms, and (right) the composite field for the growing storms. The cyclone symbol denotes the location of the center of the hurricane. The A marks the location of the upper-level anticyclone.

form over TCs. An upper-level trough is evident west of both the GI and NGI storms, but for GI storms it is stronger and extends farther south, which displaces the anticyclone a little farther east of the storm center. In addition, the winds around the anticyclone are less axisymmetric for GI storms as a result of the trough interaction. This distortion of the wind field indicates that the trough may be importing momentum into the storm. This supports earlier findings for the 200-hPa relative eddy momentum flux convergence variable, which measured greater 200-hPa momentum flux in GI storms (4.4 m s^{-1} day^{-1}) than in NGI storms (3.0 m s^{-1} day^{-1}).[2]

The 850-hPa wind fields for NGI and GI (Fig. 8) storms are dominated primarily by storm flow. Weak anticyclonic circulations directly north of NGI storms and northwest of GI storms indicate that intensifying TCs are typically south of the North Atlantic subtropical ridge. The GI cases appear to be located in a break in the subtropical ridge.

Given the presence of a stronger upper-level trough, which has been shown to displace the upper-level anticyclone, a greater magnitude of deep vertical shear is expected for GI versus NGI storms. A contour plot of differences in the mean shear of GI from NGI storms (Fig. 9) supports this. The shear is greater northeast of GI versus NGI storms.

Weakening storms have similar 200-hPa, 850-hPa, and deep-shear fields (not shown). However, the differences between GW and NGW cases are universally opposite to those of intensifying cases.

Thus there may be an optimal value of vertical shear for storm growth. For very low values, the convection is confined to the storm center, so intensification occurs without growth (the typical case). When the shear is a little higher, as in the GI anomalous case, the convection is a little less symmetric and there is greater convection outside the main eyewall. These storms continue to intensify, but also to grow. When the shear is too high, storms do not intensify or grow (as in the anomolous NGW cases).

The 700-hPa temperature advection ($-\mathbf{V} \cdot \nabla\mathbf{T}$) fields are computed using 700-hPa horizontal wind and temperature fields to determine significant differences in the baroclinic environments. Positive temperature advection values represent regions of warm air advection (WAA) and negative values cold air advection (CAA).

The 700-hPa temperature advection fields for GI storms show an interesting temperature advection dipole with strong WAA in the northeast quadrant and CAA in the northwest quadrant (Fig. 10, right). This dipole feature is not evident in NGI storm temperature advection fields (Fig. 10, left), which suggests that this highly baroclinic environment is a factor for growth in intensifying storms. A strikingly similar temperature advection dipole feature is also present for NGW

[2] The 100–600-km average 200-hPa planetary/earth eddy momentum flux convergence variable was considered, motivated by Merrill's (1984) considerations of earth angular momentum contributions to TC size. Statistical testing determined that the differences in the variable were insignificant for growing versus nongrowing storms in each intensification regime.

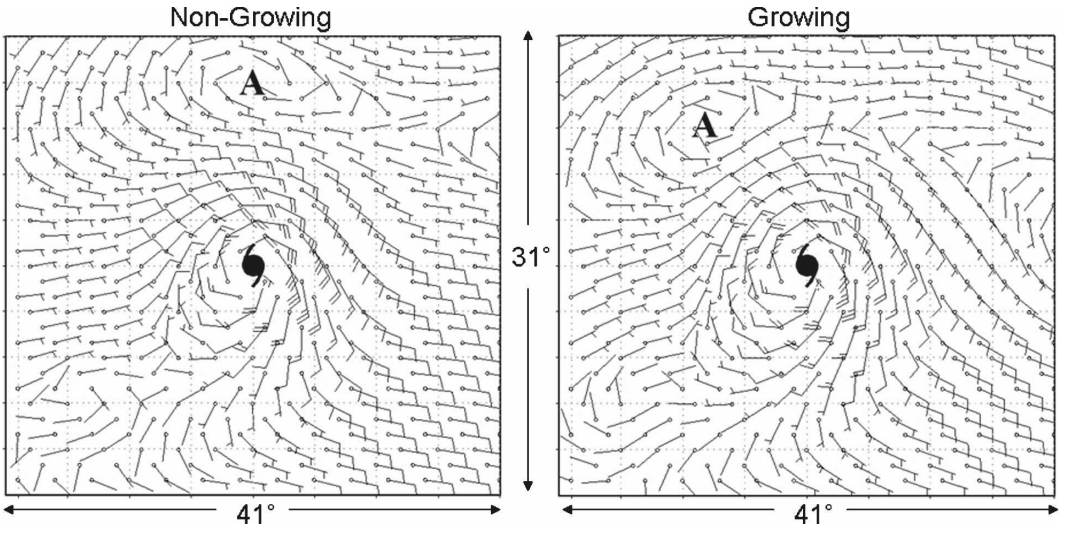

FIG. 8. The 850-hPa mean wind fields (kt) for intensifying storms. (left) The composite field for the nongrowing storms, and (right) the field for the growing storms. The cyclone symbol denotes the location of the center of the hurricane. The A marks the location of the anticyclone circulation associated with the North Atlantic subtropical ridge.

storms (not shown), implying that similar baroclinic effects influence these storms. However, the effect with respect to growth is opposite for weakening storms. The dipole in Fig. 10 suggests rising motion east of the storm center for GI cases. This result is consistent with the GOES IR standard deviation differences, which showed that these storms have more asymmetric convection away from storm center. These characteristics could be symptomatic of the initial stages of extratropical transition. Studies have shown that during extratropical transition, TCs become more convectively asymmetric and experience increased translation speed, decreased intensity, as well as an expansion in their wind fields as they travel into the more highly sheared, baroclinic midlatitudes (Sinclair 2002; Klein et al. 2000; Jones et al. 2003). Furthermore, interactions with upper-level troughs become more likely as TCs move toward the midlatitudes. However, to better understand the causes and effects of the temperature-advection dipole feature prevalent in both anomalous storm types, further study is necessary through a complete energy budget analysis.

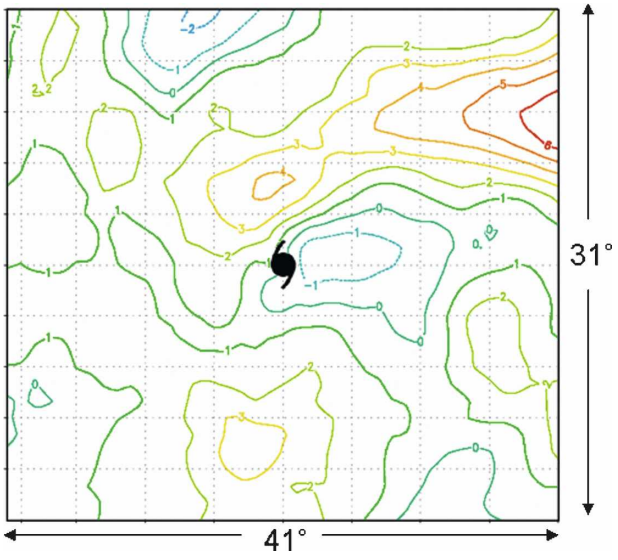

FIG. 9. The difference in the mean 850–200-hPa shear ($m\ s^{-1}$) fields (growing − nongrowing) for intensifying storms. The cyclone symbol denotes the location of the center of the hurricane.

d. Summary of mechanisms for tropical cyclone growth

The results of statistical testing and subsequent analysis imply that there are two primary ways for storms to grow. The first is growth through secondary eyewall formation, which was identified and discussed in section 4 as a mechanism for storm growth. The second type of growth is induced by environmental forcing. Environmental forcing can be caused by momentum flux from trough interactions, a more highly sheared environment, temperature advection, or a combination of these features. When a storm is in a stage of intensification, trough interaction may import additional momentum into the core, inducing growth. The baroclinicity of the storm environment can also be a source of forcing. TC development is generally thought to require a vertically stacked (barotropic) structure.

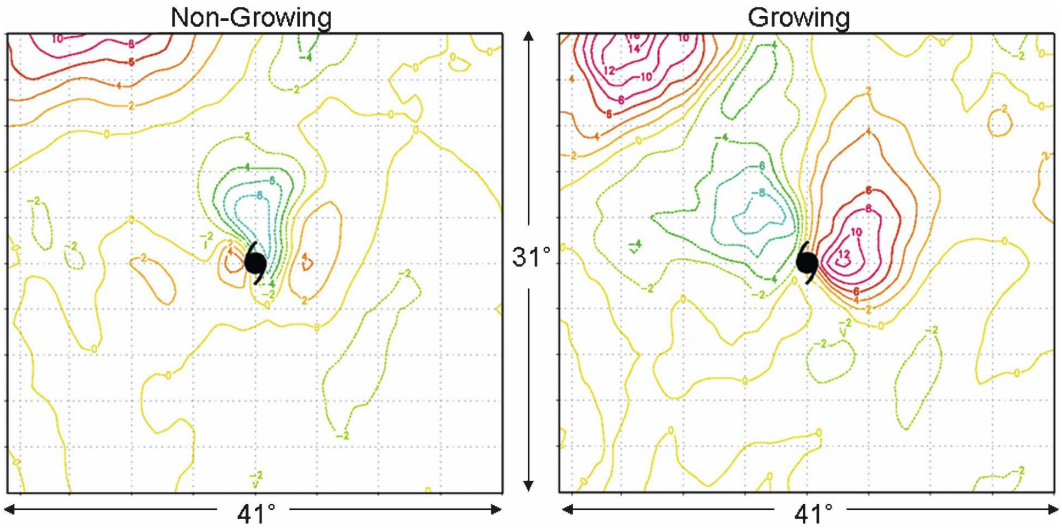

FIG. 10. The 700-hPa mean temperature advection (K s^{-1}) fields for (left) intensifying, nongrowing and (right) growing storms. The cyclone symbol denotes the location of the center of the hurricane.

However, the formation of a more tilted (baroclinic) vertical structure may cause growth by stimulating convection via heating outside of the symmetric inner core. This is suggested by the greater convective asymmetry in GI storms extending out from the eyewall. Vertical tilt is a likely result of shear from a trough or some other atmospheric disturbance. Shear can cause baroclinic instability, and hence temperature advections with flow across a temperature gradient. In this situation, potential energy from the baroclinic instability might be converted into kinetic energy in the storm leading to growth.

Environmentally forced growth applies only to storms that are in an intensification stage. For weakening storms, environmental forcing has a negative effect on structure. Recall the mean values of deep shear (SHR) for intensifying and weakening storms in Table 5. The environmental shear for both GW and GI is comparable (8.4 and 8.5 m s^{-1}, respectively). However, for NGW storms, the shear is a notably higher 9.8 m s^{-1}. Thus, moderate environmental forcing may result in storm growth; however, too much forcing can cause complete storm decay.

6. Case studies

Having determined through statistical analysis the common features and characteristics for various types of storm structural evolution, validation of these results is in order. Three storms have been chosen based on the categorization of the analyses for each storm. These cases present examples of typical and atypical structural evolution. Time series of the storm's intensity, KE′, environmental shear, and 200-hPa eddy momentum flux convergence are compared with the synoptic analysis for each storm. The shear and eddy momentum flux convergence variables are chosen because they are good indicators of possible environmental forcing.

a. Hurricane Mitch (1998)

Hurricane Mitch (1998) experienced a fairly typical structural evolution. Figure 11 shows the time series of intensity (m s^{-1}), environmental shear (m s^{-1}), 200-hPa eddy momentum flux convergence (m s^{-1} day^{-1}), and KE′ (10^6 J) for the storm, as well as the storm track from the NHC best-track data. The analyses correspond to 1800 UTC 23 October to 1200 UTC 29 October 1998. The time series plots show that from 1800 UTC 23 October to 1200 UTC 26 October 1998, the analyses categorize the storm as NGI, and during the period 0600 UTC 27 October to 1200 UTC 29 October 1998, as GW. The KE′ time series essentially mirrors the intensity time series illustrating the growth and nongrowing pattern through the storm's intensification and weakening stages. The intensifying stage indicated by the analyses encompasses the time shortly before the storm became a hurricane, located to the southwest of Jamaica, until it reached maximum intensity on the 26th. During this time, it underwent rapid intensification. A reported symmetric, well-established upper-tropospheric outflow pattern evident in satellite imagery is suggestive of a low-shear, undisruptive synoptic environment, which allowed a typical intensification process (Pasch et al. 2001). On the 27th, the storm

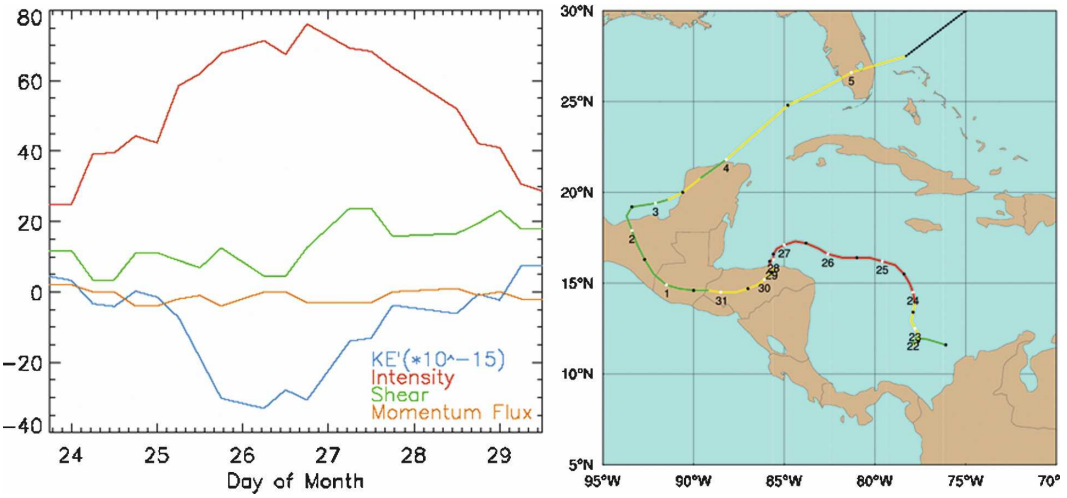

FIG. 11. (left) Time series of the intensity (m s^{-1}), environmental shear (m s^{-1}), 200-hPa eddy momentum flux convergence (m s^{-1} day^{-1}), and KE deviations (10^{16} J) from the mean curve for Hurricane Mitch (1998) and (right) the storm's track through its entire lifetime from NHC best-track data. The time series plot corresponds to the storm's track over the Caribbean Sea. The colors indicate the storm's intensity, and the numbered data points correspond to day of the month.

passed over Swan Island, shear increased, and the storm began to weaken in intensity, a process that would continue through the 29th when it made landfall in Honduras. The minimal values of eddy momentum flux convergence indicate that it did not experience much environmental forcing. Aside from land interactions, which were likely a crucial factor in the storm's weakening stages, Mitch was in an environment well suited to host a substantial TC.

b. *Hurricane Dennis (1999)*

Hurricane Dennis (1999) was an atypical storm that experienced trough interactions that appear to have enhanced the storm's structural evolution. The time series of intensity (m s^{-1}), environmental shear (m s^{-1}), 200-hPa eddy momentum flux convergence (m s^{-1} day^{-1}), and KE′ (10^6 J), as well as the storm track, are shown in Fig. 12. The analyses correspond to 0000 UTC 25 August to 1200 UTC 31 August 1999. Dennis formed 26 August in the western Atlantic at the east-southeast end of a trough and in upper-level westerly shear (Lawrence et al. 2001). This environment caused convective asymmetries in the storm with a greater amount in its eastern portion, and it prevented the storm's circulations from consolidating, as is normally seen in TCs, keeping the RMW fairly large throughout the storm's initial intensification. The increasing shear and eddy momentum flux convergence in the first portion of Fig. 12 were caused by the initial trough interaction. During this period, the KE′ also increased, indicating a growth of the wind field. The shear decreased late on the 27th, after which the storm reached its peak intensity of 46 m s^{-1} on the 28th. However, a second midlatitude trough interaction on the 28th and 29th caused a more northward movement of the storm. During this time, the RMW in the storm remained large [extending 70–85 n mi (129.6–157.4 km) 29–30 August]. This second trough interaction is evident in the time series plots of the shear and eddy momentum flux convergence. Even with increased shear and momentum flux, the storm maintained and even increased intensity, although at a fairly slow rate in comparison with Hurricane Mitch. Furthermore, the KE′ increased as well during this period as the storm's circulation grew.

c. *Hurricane Wilma (2005)*

The structural evolution of Hurricane Wilma (2005) can be separated into two stages: a first stage when the structure was controlled by internally dominated processes and a second when it was more influenced by environmental forcing. The time series of intensity (m s^{-1}), environmental shear (m s^{-1}), 200-hPa eddy momentum flux convergence (m s^{-1} day^{-1}), and KE′ (10^6 J), as well as the storm track, are shown in Fig. 13. The analyses correspond to 1800 UTC 17 October to 0000 UTC 25 October. During the first stage, while the storm was in the Caribbean, it intensified and grew through an ERC, as described in detail in section 4. This ERC, which occurred on 18–19 October, is clearly evident on the KE′ and intensity time series as a large

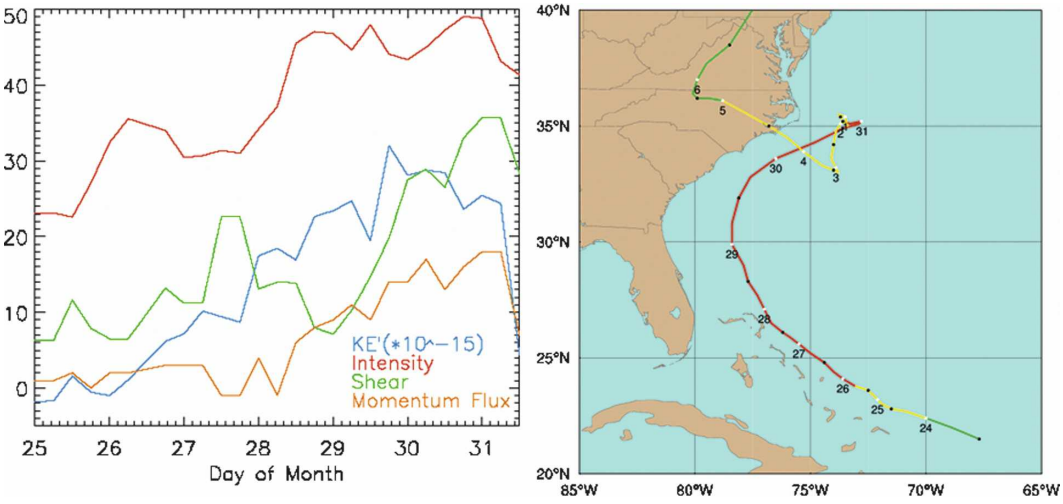

FIG. 12. (left) Time series of the intensity (m s^{-1}), environmental shear (m s^{-1}), 200-hPa eddy momentum flux convergence (m s^{-1} day^{-1}), and KE deviations (10^{16} J) from the mean curve for Hurricane Dennis (1999) and (right) the storm's track through its entire lifetime from NHC best-track data. The colors indicate the storm's intensity, and the numbered data points correspond to day of the month.

increase and moderate decrease in intensity and a corresponding large decrease and increase in KE′. As the storm traveled over the Gulf of Mexico toward and across southern Florida, it continued to grow and intensify; however, this development was a result of synoptic forcing. A strong midtropospheric trough that steered the storm along this path also created a strongly sheared environment (Pasch et al. 2006). The trough interactions during the storm's passage over the Gulf of Mexico are evident by the increasing shear and eddy momentum flux in the latter part of the time series plots. During this time, however, the storm continued to intensify and maintain and even increase a bit in size, as is demonstrated by the KE′ trend. This supports the hypothesis that trough interactions and more highly sheared environments can induce growth provided that they are not so strong as to cut off the intensification process.

7. Conclusions and future work

The overall impact of a tropical cyclone is highly dependent on the surface wind structure. To study this,

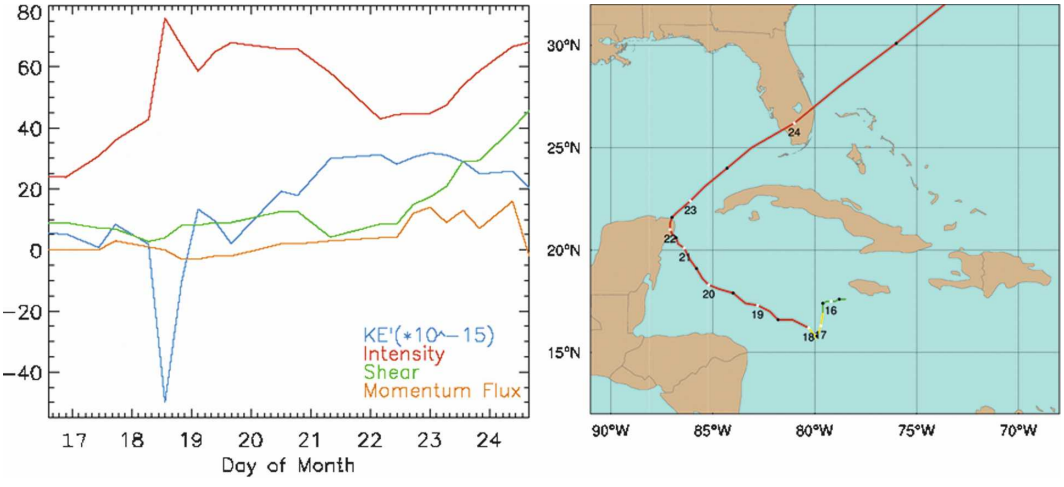

FIG. 13. (left) Time series of the intensity (m s^{-1}), environmental shear (m s^{-1}), 200-hPa eddy momentum flux convergence (m s^{-1} day^{-1}), and KE deviations (10^{16} J) from the mean curve for Hurricane Wilma (2005) and (right) the storm's track through its entire lifetime from NHC best-track data. The colors indicate the storm's intensity and the numbered data points correspond to day of the month.

the 0–200-km integrated kinetic energy data recorded from 1995–2005 of Atlantic and east Pacific TCs have been used to establish a climatology of TC KE. A new KE hurricane scale has been presented, which shows promising results in predicting TC destructive potential when applied to U.S. landfalling hurricanes from 1995–2005. This KE scale supplements the Saffir–Simpson hurricane scale by more accurately representing the destructiveness of TCs. A study of the trends in the KE with respect to intensity and structure demonstrated that TCs either intensify and do not grow or weaken and grow. Occasionally, however, a storm deviates from this evolution and grows in a stage of intensification or doesn't grow during a weakening stage. To better understand the factors behind growth in storms in different stages of intensity change, statistical testing determined significant differences between growing and nongrowing storms for a wide range of variables. Collectively, these studies provide an idea of the underlying mechanisms responsible for storm growth.

Two main types of growth mechanisms for intensifying TCs were identified. The first method was through secondary eyewall formation and subsequent ERC. During an ERC, storms initially lose intensity as the inner eyewall breaks down and is replaced by an existing secondary eyewall. The new, larger eye may contract as the storm reintensifies but generally remains larger than the previous eye. The result is an overall storm growth. The second mechanism for growth was via environmental forcing. Forcing can be caused by momentum flux from a trough interaction in which flow from an approaching trough imports momentum into the storm environment and increases the wind field. Another source of forcing could be from baroclinic effects of a sheared environment and/or temperature advection in the near-storm environment. A vertically sheared environment can cause convection to be displaced to outer regions of the storm. Similarly, the advection of warm air into a storm will lead to enhanced convection in these regions. An increase in convection in the external regions of the inner core and into the outer core can cause an overall growth for an intensifying storm.

It is interesting to note that the conditions that create an environment most suitable for growth in an intensifying storm have the opposite effect on the growth of a weakening storm. In the absence of environmental forcing, a storm will develop in a typical manner (NGI and GW), and with moderate forcing a storm may intensify and significantly increase its wind field (GI). However, storms cannot sustain intensity or their wind fields if there is too much environmental forcing (NGW). Essentially, these conditions disrupt the normal structural evolution causing a storm to evolve in an atypical manner, such that an intensifying storm will grow and a weakening storm will fall apart.

To gain a more substantial understanding of the causes of growth in a TC, further investigations are necessary. First, a more thorough look at the convective structure using the 2D GOES IR T_b profiles would provide a way to determine the location of convective asymmetries. This is of particular interest in studying NGW storms and GI storms, both of which have more asymmetric convection than their G/NG counterparts.

The next step is to carry out a full modeling study to better understand TC structure change. The observed KE evolution of a few specific TCs in the 1995–2005 dataset, representing both types of structural evolution as well as the mechanisms that may contribute to TC structural change, could be compared with Weather Research and Forecasting (WRF) Model simulations of those storms. Furthermore, a complete energy budget calculation using a model study would help determine the mechanisms behind TC growth. This information could be used to develop a prediction system for storm structure change. Such a prediction system would be a valuable tool for providing more accurate warnings to those areas in danger during the TC seasons.

Acknowledgments. This research was sponsored by CIRA activities and participation in the GOES Improved Measurement Product Assurance Plan (GIMPAP) under NOAA Cooperative Agreement NA17RJ1. The authors thank Wayne Schubert and three anonymous reviewers for providing comments that improved this manuscript. Views, opinions, and findings in this report are those of the authors and should not be construed as an official NOAA and/or U.S. government position, policy, or decision.

REFERENCES

AMS, 1993: Policy Statement: Hurricane detection, tracking, and forecasting. *Bull. Amer. Meteor. Soc.,* **74,** 1377–1380.

Brown, D., and J. Franklin, 2004: Dvorak tropical cyclone wind speed biases determined from reconnaissance-based "Best Track" data (1997–2003). Preprints, *26th Conf. on Hurricanes and Tropical Meteorology,* Monterey, CA, Amer. Meteor. Soc., 3D.5. [Available online at http://ams.confex.com/ams/26HURR/techprogram/paper_75193.htm.]

Challa, M., and R. Pfeffer, 1980: Effects of eddy fluxes of angular momentum on model hurricane development. *J. Atmos. Sci.,* **37,** 1603–1618.

Cocks, S., and W. Gray, 2002: Variability of the outer wind profiles of western North Pacific typhoons: Classification and techniques for analysis and forecasting. *Mon. Wea. Rev.,* **130,** 1989–2005.

Croxford, M., and G. Barnes, 2002: Inner-core strength of Atlantic tropical cyclones. *Mon. Wea. Rev.,* **130,** 127–139.

DeMaria, M., J.-J. Baik, and J. Kaplan, 1993: Upper-level eddy angular momentum fluxes and tropical cyclone intensity change. *J. Atmos. Sci.,* **50,** 1133–1147.

——, M. Mainelli, L. Shay, J. Knaff, and J. Kaplan, 2005: Further improvements to the Statistical Hurricane Intensity Prediction Scheme (SHIPS). *Wea. Forecasting,* **20,** 531–543.

Franklin, J., R. Pasch, L. Avila, J. Beven, M. Lawrence, S. Stewart, and E. Blake, 2006: Atlantic hurricane season of 2004. *Mon. Wea. Rev.,* **134,** 981–1025.

Hart, R., and J. Evans, 2001: A climatology of the extratropical transition of Atlantic tropical cyclones. *J. Climate,* **14,** 546–564.

Holland, G., and R. Merrill, 1984: On the dynamics of tropical cyclone structural changes. *Quart. J. Roy. Meteor. Soc.,* **110,** 723–745.

Jones, S., and Coauthors, 2003: The extratropical transition of tropical cyclones: Forecast challenges, current understanding, and future directions. *Wea. Forecasting,* **18,** 1052–1092.

Kantha, L., 2006: Time to replace the Saffir-Simpson Hurricane Scale? *Eos, Trans. Amer. Geophys. Union,* **87,** 1, doi:10.1029/2006EO010003.

Kimball, S., and J. Evans, 2002: Idealized numerical simulations of hurricane-trough interactions. *Mon. Wea. Rev.,* **130,** 2210–2227.

——, and M. Mulekar, 2004: A 15-year climatology of North Atlantic tropical cyclones. Part I: Size parameters. *J. Climate,* **17,** 3555–3575.

Kistler, R., and Coauthors, 2001: The NCEP–NCAR 50-Year Reanalysis: Monthly means CD-ROM and documentation. *Bull. Amer. Meteor. Soc.,* **82,** 247–267.

Klein, P., P. Harr, and R. Elsberry, 2000: Extratropical transition of western North Pacific tropical cyclones: An overview and conceptual model of the transformation stage. *Wea. Forecasting,* **15,** 373–395.

Knabb, R., J. Rhome, and D. Brown, cited 2006: Tropical cyclone report: Hurricane Katrina, 43 pp. [Available online at http://www.nhc.noaa.gov/pdf/TCR-AL122005_Katrina.pdf.]

Kossin, J., 2002: Daily hurricane variability inferred from GOES infrared imagery. *Mon. Wea. Rev.,* **130,** 2260–2270.

Lawrence, M., L. Avila, J. Beven, J. Franklin, J. Guiney, and R. Pasch, 2001: Atlantic hurricane season of 1999. *Mon. Wea. Rev.,* **129,** 3057–3084.

Merrill, R. T., 1984: A comparison of large and small tropical cyclones. *Mon. Wea. Rev.,* **112,** 1408–1418.

Molinari, J., and D. Vollaro, 1989: External influences on hurricane intensity. Part I: Outflow layer eddy angular momentum fluxes. *J. Atmos. Sci.,* **46,** 1093–1105.

Mueller, K., M. DeMaria, J. Knaff, and T. H. Vonder Haar, 2006: Objective estimation of tropical cyclone wind structure from infrared satellite data. *Wea. Forecasting,* **21,** 990–1005.

Pasch, R., L. Avila, and J. Guiney, 2001: Atlantic hurricane season of 1998. *Mon. Wea. Rev.,* **129,** 3085–3123.

——, E. Black, H. Cobb, and D. Roberts, cited 2006: Tropical cyclone report: Hurricane Wilma, 27 pp. [Available online at http://www.nhc.noaa.gov/pdf/TCR-AL252005_Wilma.pdf.]

Powell, M., and T. Reinhold, 2007: Tropical cyclone destructive potential by integrated kinetic energy. *Bull. Amer. Meteor. Soc.,* **88,** 513–526.

——, S. Houston, L. Amat, and N. Morisseau-Leroy, 1998: The HRD real-time hurricane wind analysis system. *J. Wind Eng. Ind. Aerodyn.,* **77–78,** 53–64.

Shapiro, L., and H. Willoughby, 1982: The response of balanced hurricanes to local sources of heat and momentum. *J. Atmos. Sci.,* **39,** 378–394.

Sinclair, M., 2002: Extratropical transition of southwest Pacific tropical cyclones. Part I: Climatology and mean structure changes. *Mon. Wea. Rev.,* **130,** 590–609.

Toth, Z., E. Kalnay, S. Tracton, R. Wobus, and J. Irwin, 1997: A synoptic evaluation of the NCEP ensemble. *Wea. Forecasting,* **12,** 140–153.

Wang, Y., and C.-C. Wu, 2004: Current understanding of tropical cyclone structure and intensity changes—A review. *Meteor. Atmos. Phys.,* **87,** 257–278.

Weatherford, C., and W. M. Gray, 1988a: Typhoon structure as revealed by aircraft reconnaissance. Part I: Data analysis and climatology. *Mon. Wea. Rev.,* **116,** 1032–1043.

——, and ——, 1988b: Typhoon structure as revealed by aircraft reconnaissance. Part II: Structural variability. *Mon. Wea. Rev.,* **116,** 1044–1056.

Willoughby, H., J. Clos, and M. Shoreibah, 1982: Concentric eye walls, secondary wind maxima, and the evolution of the hurricane vortex. *J. Atmos. Sci.,* **39,** 395–411.